Disengaging the Smc3/kleisin interface releases cohesin from *Drosophila*chromosomes during interphase and mitosis

Christian S Eichinger[1*], Alexandre Kurze[1*], Raquel A Oliveira[1†] and Kim Nasmyth[1, a]

[a]Department of Biochemistry, University of Oxford, South Parks Road, Oxford OX1 3QU, UK. Tel.:+44 186 561 3229; Fax:+44 186 561 3341; E-mail: kim.nasmyth@bioch.ox.ac.uk

[*]These authors contributed equally to this work

[†]Present address: Instituto Gulbenkian de Ciência, Oeiras, Portugal.

ABSTRACT

Cohesin's Smc1, Smc3, and kleisin subunits create a tripartite ring within which sister DNAs are entrapped. Evidence suggests that DNA enters through a gate created by transient dissociation of the Smc1/3 interface. Release at the onset of anaphase is triggered by proteolytic cleavage of kleisin. Less well understood is the mechanism of release at other stages of the cell cycle, in particular during prophase when most cohesin dissociates from chromosome arms in a process dependent on the regulatory subunit Wapl. We show here that Wapl-dependent release from salivary gland polytene chromosomes during interphase and from neuroblast chromosome arms during prophase is blocked by translational fusion of Smc3's C-terminus to kleisin's N-terminus. Our findings imply that proteolysis-independent release of cohesin from chromatin is mediated by Wapl-dependent escape of DNAs through a gate created by transient dissociation of the Smc3/kleisin interface. Thus, cohesin's DNA entry and exit gates are distinct.

Keywords: cohesin, *Drosophila melanogaster*, prophase pathway, sister chromatid cohesion, Wapl

INTRODUCTION

Cohesin is a multisubunit complex with numerous roles throughout the genomes of all eukaryotic cells (Hirano, 2006; Peters et al, 2008; Nasmyth and Haering, 2009). By holding sister DNAs together from S phase until the onset of anaphase, cohesin is essential for chromosome segregation during mitosis and both meiotic divisions. It is also important for the repair of double-strand breaks in post-replicative cells and for regulating the structure and transcription of interphase chromosomes in quiescent as well as dividing cells (Dorsett and Strom, 2012). Defects in cohesin function have been implicated in age-related chromosome missegregation in oocytes (Lister et al, 2010), in numerous types of tumours (Mannini and Musio, 2011), and in at least two genetic syndromes, namely Cornelia de Lange and Roberts syndrome (Liu and Krantz, 2008; Dorsett and Krantz, 2009).

At the heart of the cohesin complex is a tripartite ring created by pairwise interactions between its Smc1, Smc3, and α-kleisin subunits (Haering et al, 2002; Gruber et al, 2003). Smc1 and Smc3 are related rod-shaped proteins whose 50 nm long intra-molecular coiled coils contain a dimerization domain at one end and an ABC (*A*TP *B*inding *C*assette)-like ATPase head domain composed of N- and C-terminal domains at the other. Heterotypic interactions between the dimerization domains create V-shaped heterodimers with ‘hinges' at their base and Smc1 and Smc3 ATPase heads at their vertices. The latter are subsequently bound by the C- and N-terminal domains respectively of α-kleisin subunits, known as Scc1 or Rad21 in animal cells.

Cohesin rings are thought to act as topological devices that entrap DNA molecules (Haering et al, 2008). This notion, known as the ring model, supposes that the association between cohesin and chromosomes arises from entrapment of individual chromatin fibres while sister chromatid cohesion from co-entrapment of sister DNAs. Cohesin's *de novo* association with chromatin requires a regulatory subunit known as Scc3/SA (Hu et al, 2011) that binds to α-kleisin's central domain, hydrolysis of ATP bound to both Smc1 and Smc3 NBDs (Hu et al, 2011), and a separate ‘loading' complex called kollerin (Nasmyth, 2011) composed of a HEAT repeat-containing protein Scc2 (Nipped-B in *Drosophila melanogaster*) bound to a TPR (*T*etratrico *P*eptide *R*epeat) protein called Scc4 (Ciosk et al, 2000; Nasmyth, 2011).

If loading cohesin onto chromosomes involves entrapment of DNAs inside cohesin rings, then it presumably requires creation of a DNA entry gate created through transient dissociation of one of the ring's three inter-subunit interfaces. The fact that cohesin remains functional following translational fusion of kleisin's N- and C-terminal domains to Smc3 and Smc1's C-terminal and N-terminal domains, respectively, excludes Smc/kleisin interfaces as obligatory entry gates (Gruber et al, 2006). In contrast, artificial tethering of Smc1 and Smc3 hinge domains interferes with the

establishment of sister chromatid cohesion (Gruber et al, 2006), suggesting that DNA enters the ring via its Smc1/3 interface.

Cohesin's subsequent release from chromatin occurs via two independent mechanisms. The first and best understood involves proteolytic cleavage by separase of the central domain of cohesin's kleisin subunit, which triggers immediate dissociation from chromatin and loss of sister chromatid cohesion at the metaphase to anaphase transition (Nasmyth and Haering, 2005). A second mechanism releases cohesin from chromatin in a separase-independent manner at other stages of the cell cycle (Waizenegger et al, 2000). This process is especially active during prophase and pro-metaphase, when most cohesin dissociates from chromosome arms in a process known as the prophase pathway. The prophase pathway was initially identified in *Xenopus* (Losada et al, 1998) and involves phosphorylation of Scc3/SA subunits by mitotic protein kinases such as PLK (Losada et al, 2002; Sumara et al, 2002; Gimenez-Abian et al, 2004; Hauf et al, 2005). Shugoshin proteins protect centromeric cohesin from the prophase pathway, probably by recruiting PP2A (Riedel et al, 2006; Xu et al, 2009).

Cohesin's release from chromosomes in a separase-independent manner depends on Wapl, a protein originally identified by genetic studies in *Drosophila* and subsequently found associated with cohesin in mammalian cells (Verni et al, 2000; Gandhi et al, 2006; Kueng et al, 2006). Wapl is recruited to yeast cohesin by binding a HEAT repeat containing regulatory subunit called Pds5, which binds to tripartite rings close to α-kleisin's N-terminal domain (Chan et al, 2012), though additional Wapl-recruiting mechanisms may exist in *Xenopus* (Shintomi and Hirano, 2009). In addition to Wapl, releasing activity in yeast involves a pair of highly conserved lysines on Smc3 NBDs (K112 and K113), two specific domains within Scc3, and a specific domain within Pds5 additional to that required to recruit Wapl itself (Chan et al, 2012). The process of release must therefore be a complex one.

Crucially, formation of cohesion between sister chromatids stable enough to facilitate chromosome segregation depends on marking a subset of cohesin complexes in a manner that causes them to be refractory to releasing activity. This is achieved by the modification during S phase of K112 and K113 by the Eco1 acetyl transferase (Ivanov et al, 2002; Ben-Shahar et al, 2008; Unal et al, 2008; Rowland et al, 2009), which in animal cells recruits a protein called sororin that alters the association between Wapl and Pds5 (Nishiyama et al, 2010).

If separase releases cohesin from chromatin by enabling DNAs to escape from rings cleaved open by kleisin cleavage, then non-proteolytic release may achieve the same goal by dissociating transiently one of the tripartite ring's three inter-subunit interfaces. By showing that cohesin associated with interphase chromatin in *Drosophila* salivary glands is released within minutes of cleavage of kleisin using TEV protease, even in cells lacking Wapl, we provide evidence that all chromosomal

cohesin and not just that conferring cohesion is topologically associated. If so, then physiological release must also involve creation of an exit gate. To test the suggestion that this is located at the Smc3/kleisin interface (Nasmyth, 2011), we analysed the effect on cohesin dynamics of fusing Smc3's C-terminal domain to the N-terminal of kleisin. Remarkably, we found that this blocks Wapl-dependent release from individual loci within polytene chromosomes as well as from chromosome arms during prophase in proliferating neuroblasts. Our results imply that cohesin's dissociation from chromatin during both interphase and prophase is driven by the same mechanism, one that involves transient opening of the Smc3/kleisin interface. By elucidating the mechanism of release during prophase and by demonstrating an effect of Wapl on cohesin's release from individual loci within minutes of cleaving a linker connecting Smc3 and α-kleisin, our work is a major extension of related experiments recently reported in yeast (Chan et al, 2012). Our results imply that cohesin has separate gates for DNA entry and exit and provide a mechanistic basis for understanding the distribution of cohesin throughout eukaryotic genomes.

RESULTS

Cohesi is dynamic at specific loci on polytene chromosomes

Little is known about the properties of cohesin's association with specific loci during interphase. Is it topological and how rapidly does it turnover? To address these questions, we used confocal microscopy to image in living salivary gland cells from *Drosophila melanogaster* a GFP-tagged version of cohesin's kleisin subunit that contains TEV-protease recognition sites (Rad21(TEV)-GFP). The advantage of this tissue is that it is composed of non-dividing transcriptionally active cells whose polytene chromosomes each contain 1024 identical DNA molecules bundled together in close alignment. Rad21(TEV)-GFP was expressed from a transgene under control of a tubulin pomoter in stocks whose endogenous Rad21 locus had been excised. Live-cell imaging of dissected salivary glands revealed Rad21(TEV)-GFP's association with numerous loci (Figure 1A). We used the rate of fluorescence recovery after photobleaching (FRAP) to measure turnover kinetics at several of the more prominent bands (Figure 1B). Their rates of recovery were similar, with half lives around 40 s (Figure 1C; Supplementary Movie S1). Imaging of a GFP-tagged version of cohesin's Smc3 subunit revealed similar turnover kinetics (Supplementary Movie S2), which is in agreement with previous FRAP data of Smc1-GFP (Gause et al, 2010). To address the physical nature of cohesin's association with polytene loci, we microinjected into the cytoplasm of the salivary gland cells active or inactive versions of TEV protease containing an NLS and then followed the fate of Rad21(TEV)-GFP by live-cell imaging. The active version abolished Rad21(TEV)-GFP's association with specific loci within 2–4 min (Figure 1D; Supplementary Movies S3 and S4). Given the rapid turnover of cohesin on polytene chromosomes, it

is not possible to ascertain whether TEV-induced kleisin cleavage triggers cohesin's dissociation from chromatin or whether it merely abolishes re-loading.

Cohesin's turnover on polytene chromosomes depends on Wapl

To test whether Wapl has a role in the turnover of cohesin in non-dividing tissues, we analysed the distribution and turnover of Rad21(TEV)-GFP on polytene chromosomes within salivary gland cells isolated from mutant stocks hemizygous for *wapl*^{C204} (Verni et al, 2000). Though *wapl*^{C204} is probably a null allele and causes lethality at the third-instar larvae state, salivary gland cell endoduplication proceeds normally, presumably due to the inheritance of maternal gene product. Cohesin still localizes to specific bands in *wapl*^{C204} salivary gland cells, but their morphology is significantly different to those in wild type. The banding pattern is more pronounced throughout the genome, many bands appear bent or circular, and the soluble pool of cohesin is greatly reduced (Figure 2A). Strikingly, turnover was greatly diminished (Figure 2B and C). For most chromosomal cohesin in *wapl*^{C204} cells, there was imperceptible turnover within a several minute interval.

To address whether the lack of turnover is due to entry of *wapl*^{C204} cells into a pathological state in which turnover has been switched off, we analysed the effect of microinjecting mRNA encoding wild-type Wapl. This caused a major reduction in the amount of Rad21(TEV)-GFP associated with specific bands and the accumulation of a more pronounced soluble pool (Figure 2D). Importantly, cohesin associated with specific bands following Wapl restoration turned over with kinetics similar to that in wild-type cells (Supplementary Movie S5). The immediate resumption of cohesin turnover following Wapl re-activation implies that the lack of turnover in *wapl*^{C204} cells is caused directly by the lack of Wapl and not by any altered developmental fate. The increased proportion of chromosomal cohesin associated with specific bands as well as with its greatly reduced turnover in *wapl*^{C204} cells implies that Wapl has a crucial role in releasing cohesin from polytene chromosomes. Injection of active but not inactive TEV protease rapidly abolished Rad21(TEV)-GFP bands in *wapl*^{C204} cells with similar kinetics to wild type (Figure 2E;Supplementary Movies S6 and S7). This implies that kleisin cleavage triggers cohesin's immediate dissociation from chromatin even in the absence of Wapl-mediated turnover, a finding consistent with the notion that cohesin's chromosomal association is topological.

Cohesin whose Smc3/kleisin interface cannot be disengaged loads onto polytene chromosomes

If cohesin associates with polytene chromosomes through entrapment of chromatin fibres within its tripartite ring, albeit in a locus-specific manner, then it follows that Wapl-promoted release must involve their escape through an opening created by dissociation of one of the tripartite ring's three inter-subunit interfaces. To test the suggestion that cohesin's DNA exit gate resides where kleisin's N-terminal domain

binds to Smc3's NBD (Nasmyth, 2011), we investigated the effect of linking Smc3's C-terminus to kleisin's N-terminus. To do this, we generated transgenic flies that express a GAL4-inducible Smc3-Rad21-GFP fusion protein (Figure 3A) in which Smc3 and Rad21 are covalently connected through a 50 amino acid long polypeptide linker containing three tandem TEV recognition sites. The Smc3-Rad21-GFP fusion protein was expressed in an inducible manner because if our hypothesis is correct, constitutive expression should cause lethality similar to that of *wapl*^{C204} mutants. Temporal control of fusion protein expression was achieved by combining the GAL4-inducible Smc3-Rad21-GFP transgene with a heat shock-inducible GAL4. We introduced a third transgene permitting GAL4-inducible expression of an NLS-containing TEV protease, which enabled us to compare the effect of expressing the Smc3-Rad21-GFP fusion protein with and without cleavage of the linker connecting Smc3 and Rad21.

Western blotting of whole larval extracts showed that Smc3-Rad21-GFP accumulated in response to a 30 min heat shock of third-instar larvae at 37°C followed by a 7 h recovery period at 25°C (Figure 3B). In salivary glands, we found that comparable levels of fusion protein accumulated after incubation at 25°C for 3 h following a short 2 min heat shock at 37°C (Figure 3C). Immunoprecipitation of Smc3-Rad21-GFP fusion protein showed that it interacts with endogenous Smc1 but not endogenous Rad21, implying that it is incorporated into *bona fide* cohesin ring complexes (Supplementary Figure S1). The fusion protein was converted to separate Smc3 and Rad21-GFP proteins upon simultaneous induction of TEV protease (Figure 3C).

Following induction, Smc3-Rad21-GFP accumulated at numerous specific loci throughout the polytene chromosomes of *Drosophila* salivary glands (Figure 3D). In addition to forming more conventional bands, the fusion protein formed circular structures (at certain loci) that resembled those formed by Rad21(TEV)-GFP in hemizygous *wapl*^{C204} mutant cells. Crucially, these abnormal structures were not observed when TEV protease was co-expressed (Figure 4A and B). The formation of bands and circles at specific loci by intact Smc3-Rad21-GFP fusion proteins indicates that disengagement of the Smc3 NBD/kleisin interface is unnecessary for cohesin loading, as found in yeast (Gruber et al, 2006).

Cohesin whose Smc3 NBD is fused to kleisin's N-terminus fails to turnover

To address whether fusion of Smc3's C-terminus to kleisin's N-terminus alters cohesin's turnover, we briefly heat shocked third-instar larvae in the presence and absence of GAL4-inducible TEV protease and isolated their salivary glands following subsequent incubation at 25°C for 3 h. FRAP showed that cohesin containing intact Smc3-Rad21-GFP fusion protein failed to turn over. This lack of mobility can be

attributed to the linkage of Smc3 with Rad21 because cleavage of the intervening polypeptide created a sizeable pool of mobile complexes (Figure 4A and B).

Cleaving the polypeptide linking Smc3's NBD to kleisin's N-terminus triggers release

Because TEV was expressed simultaneously with Smc3-Rad21-GFP in the above experiment, most Smc3-Rad21-GFP fusion proteins will have been cleaved prior to cohesin loading. To address whether cohesin containing the fusion protein had indeed loaded in a normal manner but had merely failed to release, we tested whether it can be triggered to do so in response to TEV protease microinjection. Once sufficient Smc3-Rad21-GFP protein had associated with polytene chromosomes following a brief heat shock, we microinjected either active or inactive TEV protease into salivary gland cells and imaged GFP fluorescence in real time. This revealed that active but not inactive TEV induced rapid disappearance of fluorescence at most if not all loci. Thus, cleavage of the linker connecting Smc3 and Rad21 triggers rapid release from chromatin of cohesin containing Smc3-Rad21-GFP (Figure 5A and B; Supplementary Movies S8 and S9). To address whether the extinction of locus-specific GFP fluorescence under these circumstances is dependent on Wapl, we set up a cross that produced progeny expressing Smc3-Rad21-GFP in a wild-type or *wapl*^{C204} mutant background. Injection of TEV protease into *wapl*^{C204} salivary gland cells had little or no effect while injection into wild-type cells caused release, as expected (Figure 5C; Supplementary Movie S10). Importantly, FRAP demonstrated that cohesin containing Smc3-Rad21-GFP failed to turn over in*wapl*^{C204} salivary gland cells even when cells had been injected with TEV protease (Supplementary Movie S11). We therefore conclude that connection by a polypeptide linker of Smc3's NBD with Rad21's N-terminal domain permits cohesin loading but blocks completely its subsequent Wapl-dependent release. It was difficult to assess from these experiments whether cohesin released by Wapl upon cleavage of the Smc3-Rad21 linker is subsequently capable of reloading. We suspect that the high levels of expression in these salivary gland cells create a large pool of soluble cleaved complexes that obscure those that reassociate with specific loci.

Wapl-dependent release of cohesin from chromosome arms during prophase is blocked by linking Smc3's NBD to kleisin's N-terminus

To test whether preventing disengagement of Smc3's NBD from kleisin's N-terminal domain blocks the prophase pathway, we set out to measure this process using optical imaging of living *Drosophila*neuroblasts. To do this, we used fruit fly stocks containing a transgene expressing a fully functional GFP-tagged version of Rad21 (*Rad21-GFP*) in a background lacking the endogenous Rad21 locus (*Rad21*^{ex}). These also carried transgenes expressing either RFP tagged histone H2A (H2Av-mRFP1), to visualize whole chromosomes, or RFP-tagged CenH3 (CID-mRFP1), to visualize centromeres.

Time-lapse photo-microscopy revealed that cohesin disappeared from chromosome arms soon after nuclear envelope breakdown but remained in the vicinity of centromeres until the onset of anaphase, at which point it disappeared also from this location (Figure 6A; Supplementary Movie S12). Still images of metaphase cells whose sister kinetochores had bi-oriented revealed that cohesin is located exclusively within peri-centric chromatin flanked by sister kinetochores (Figure 6B). To our knowledge, this is the first time that dissociation of cohesin from chromosome arms but not centromeres during prophase and its sudden disappearance from centromeres at the onset of anaphase has been observed in living cells. In contrast, time-lapse photo-microscopy of neuroblasts from larvae hemizygous for *wapl*^{C204} revealed that Rad21-GFP persisted throughout the length of their chromosomes until the onset of anaphase (Figure 6C;Supplementary Movie S13), whereupon it disappeared entirely from chromosomes (Supplementary Movie S13). We conclude from these observations that a *bona fide* prophase pathway removes cohesin from chromosome arms in *Drosophila* neuroblasts while separase removes it from centromeres. Interestingly, the failure of *wapl*^{C204} neuroblasts to remove cohesin from their chromosome arms prior to the onset of anaphase does not prevent chromosome segregation, presumably because separase removes cohesin from both arms and centromeres under these circumstances (Supplementary Movie S13), a finding congruent with the behaviour of HeLa cells whose Wapl protein has been depleted by RNA inference (Kueng et al, 2006).

To address whether blocking disengagement of Smc3's NBD from kleisin prevents cohesin's release from chromosome arms during prophase, we induced Smc3-Rad21-GFP expression in third-instar larvae using a 20 min heat shock at 37°C and then allowed recovery for 8–10 h at 25°C before imaging cohesin within living neuroblasts. This revealed that cohesin containing an intact Smc3-Rad21-GFP fusion protein persisted on chromosome arms after nuclear envelope breakdown (Figure 6D). Crucially, cleavage of the linker connecting cohesin's Smc3 and kleisin subunits restored cohesin's dissociation from chromosome arms during prophase (Figure 6D). We conclude that preventing disengagement of Smc3's NBD from kleisin's N-terminal domain blocks cohesin's release from chromosome arms during prophase as well as during interphase. Our data imply that release during interphase and prophase is mediated by the same fundamental mechanism. Furthermore, they are fully consistent with the notion that this involves escape of chromatin fibres from cohesin rings due to the transient creation of an exit gate at the Smc3/kleisin interface. There is nevertheless at least one major difference between the prophase and interphase processes. Because cohesin's releasing activity may be more active during prophase, an interval during which kollerin-mediated loading is probably shut down (Hauf et al, 2005), cohesin is completely removed from chromosome arms during prophase but merely turns over during interphase.

DISCUSSION

We reveal here the first major insight into the mechanism by which Wapl catalyses release of cohesin from chromosomes in animal cells. Our finding that cohesin stably associated with polytene chromosomes in *wapl*^{C204} salivary glands immediately dissociates from them upon cleavage of its kleisin subunit by TEV protease suggests that the association is topological and involves entrapment of DNAs within cohesin's tripartite ring. An implication is that release must involve escape from this embrace. In other words, the ring must have a DNA exit gate, which must be located at one of the three interfaces between cohesin's Smc1, Smc3, and kleisin subunits. If so, then linking this interface should interfere with release. We show that cohesin complexes whose Smc3 and kleisin subunits have been replaced by a Smc3-kleisin fusion protein in which Smc3's NBD is linked by a short polypeptide to the N-terminal domain of kleisin are still capable of associating with chromatin but cannot subsequently be released. Crucially, cleavage of the linker peptide with TEV protease restores Wapl-dependent release within 2 min. Our results are consistent with the notion that cohesin associates with chromatin topologically and that Wapl-dependent release occurs through transient dissociation of kleisin's N-terminal domain from Smc3's NBD, creating a gate through which chromatin fibres escape. Our finding that cohesin's dissociation from chromosome arms as neuroblasts enter mitosis is also blocked by fusing Smc3 and kleisin implies that a similar if not identical release mechanism is responsible for the prophase pathway. Though we have not directly visualized the transient disconnection of Smc3 NBDs from kleisin's N-terminal domain, it is difficult to envisage an alternative explanation for our results.

Recent experiments conducted in parallel to those presented here (Chan et al, 2012) have shown that yeast cohesin is also capable of dissociating from chromatin in a separase-independent manner and that this activity like the equivalent process in *Drosophila* is blocked by fusion of Smc3 and kleisin. The process described here appears therefore to be a highly conserved property of the complex. Importantly, our experiments go beyond the yeast work in two important respects. Because we are able to manipulate the complex within minutes or even seconds by microinjection, we were able to demonstrate the immediate restoration of release by cleaving the linker connecting Smc3 and kleisin. Second, unlike yeast, *Drosophila*neuroblasts clearly possess a *bona fide* prophase pathway, which permitted us to demonstrate that it too was blocked by preventing disconnection of Smc3 NBDs from the N-terminal domain of α-kleisin.

The insight that cohesin associates with chromatin using a topological principle and that association is relinquished by escape of DNAs through an exit gate distinct from that used for entry has wide-ranging ramifications. It reveals that much if not most chromosomal cohesin in animal cells is in a dynamic steady state whose parameters are determined by the rates of loading and release. It is both remarkable and sad

that the precise values of these parameters have important pathological as well as biological consequences. Though heterozygosity of Nipbl (Scc2) in humans results in a mere 30% drop in the amount of kollerin, it nevertheless leads to highly pleiotropic developmental defects within many organs (Liu and Krantz, 2008). This phenomenon is easier to comprehend now that we realize that kollerin and releasing activity use different mechanisms to entrap and release DNAs, respectively, and that the fraction of cohesin associated with chromatin as well as its turnover kinetics are the product of a steady state. Our work raises the possibility that similar principles govern the association with chromatin of all other Smc/kleisin complexes. Because condensin also forms tripartite rings (Cuylen et al, 2011), we suggest that it too entraps and releases DNAs via its Smc2/4 hinge and Smc2/kleisin interfaces, respectively. A similar principle could also govern the association with DNA of eukaryotic Smc5/6 complexes as well as bacterial Smc/kleisin complexes. An important question that remains open is how Plk1 activity and phosphorylation of SA/Scc3 increases the rate of cohesin's release from chromosome arms after cells enter mitosis, which gives rise to greatly reduced cohesion and a cross-like morphology that is one of the most potent emblems of chromosome biology.

MATERIALS AND METHODS

Cloning

Rad21-GFP and Rad21(TEV)-GFP transgenes were generated based on p-element constructs described previously (Pauli et al, 2008; Oliveira *et al*, manuscript in preparation). SMC3 was amplified from cDNA (BDGB clone IP16426) and cloned into the pCaSpeR vector with 500 bp of 5′UTR and 3′UTR of the SMC3 gene. To drive expression a tubulin promotor was added by In-Fusion cloning (Clontech) upstream of the 5′UTR. An N-terminal GFP tag with a 3 × GlyAla linker was added to Smc3. The pCaSpeR UAS-Smc3-Rad21-GFP construct was obtained by replacing the tubulin promotor by a UAS sequence. The Rad21-GFP sequence including a 25 × GlyAla linker was cloned by replacing the SMC3 STOP codon by In-Fusion cloning. Smc3 and Rad21 were translationally fused by a 50 amino acid peptide linker, which includes three TEV protease recognition sites.

Fly strains

Flies were kept and maintained as described previously (Pauli et al, 2008). Fly transgenesis was carried out at BestGene company (Chino Hills, CA, USA). *Rad21-GFP* and *Rad21(TEV)-GFP* flies (Oliveira *et al*, manuscript in preparation) were recombined with flies in which endogenous Rad21 was excised ($Rad21^{ex15}$; Pauli et al, 2008) and were able to rescue the lethality of Rad21 null mutations. TEV-cleavage experiments were performed in heterozygous *Rad21(TEV)-GFP* $Rad21^{ex}$ $H2Av^{RFP}$ flies in a wild-type or hemizygous $wapl^{C204}$ background as well as in flies expressing a Smc3-Rad21-GFP fusion protein in an otherwise wild-type genetic

background. *wapl*^{C204} mutant flies were kindly provided by Maurizio Gatti's lab (Verni et al, 2000). For experiments involving X chromosome-linked *wapl*^{C204} mutants, only male flies (harbouring only one X chromosome) were used. Fly strains also expressed H2Av-mRFP1 (Schuh et al, 2007) (or polyubiquitin H2A-mRFP1, kindly provided by Jennifer Mummery-Widmer, Juergen Knoblich lab, IMBA,Vienna, Austria) to monitor DNA or CID-mRFP1 (Schuh et al, 2007) to monitor centromeres.

Heat shock induction of protein expression

For heat shock induction of GAL4-driven protein expression, crosses were set up freshly between homozygous UAS-Smc3-Rad21-GFP and hsGAL4/UAS-TEV-NLS or hsGAL4 for salivary gland as well as neuroblast experiments. Namely, virgin female flies expressing homozygous hsGAL4/UAS-TEV-NLS or hsGAL4 were crossed to male flies homozygous for a UAS-Smc3-Rad21-GFP transgene. Actively crawling progeny third-instar larvae of these crosses, which harbour exactly one of each transgene were used for the final experiments. Flies and progeny larvae were kept at 25°C under non-crowded conditions. Smc3-Rad21-GFP and TEV protease expression was induced in crawling third-instar larvae by heat shock (2 min at 37°C followed by 0–4 h at 25°C). For western blot analysis, two salivary gland pairs were dissected for each time point.

Tissue dissection and culturing

During this study, we were using two kinds of tissues of *Drosophila* third-instar larvae: salivary glands and brain tissues. Actively crawling fly larvae were collected. Salivary glands were dissected in SF9 media, fat tissue was removed and salivary glands were mounted on poly-lysine covered slides. Larval brains were dissected and cultured in Schneider media supplemented with 10% FBS and diluted 4:1 with sterile water.

Western blot analysis

Western blot analysis was performed from dissected third-instar larval salivary glands or whole larvae according to standard protocols. Larvae or dissected salivary glands were homogenized in SDS sample loading buffer and boiled for 5 min. Western blot was performed according to standard procedures. The following antibodies were used: guinea-pig α-Rad21 (1:5000) (Heidmann et al, 2004), α-Smc1 (1:2000; received from Claudio Sunkel's lab), and mouse α-tubulin (DM1 A) (1:7500; Sigma-Aldrich). HRP-linked guinea-pig (1:15 000), mouse (1:5000), and rat (1:5000) secondary antibodies (GE Healthcare) were detected by Enhanced Chemi-Luminescence (ECL) (Millipore).

Spinning disk microscopy and FRAP analysis

Time-lapse microscopy still imaging was performed with a spinning disk confocal microscope (Perkin Elmer) equipped with a 60 × Silicon Immersion Oil lense (Olympus, NA 1.35) and a Hamamatsu C9100-13 EMCCD camera at 25°C. For FRAP analysis, salivary glands were dissected in SF9 media, mounted on poly-lysine slides and covered by a membrane (YSI membrane kit) and a thin layer of 700 halocarbon oil (Halocarbon Products Corporation). Imaging settings for time-lapse microscopy, still and FRAP analysis were as followed. For the GFP channel, we used an exposure time of 100 ms, 488 nm laser power output of 15%, Sensitivity of 200, camera mode EMCCD, and FRAP 488 nm laser power output of 40%. The RFP channel was set to an exposure time of 50 ms, 561 nm laser power output of 2%, Gain 1 and Sensitivity of 60. Imaging of neuroblasts was performed with 200 ms exposure time, Sensitivity 165 and 488 nm laser power 20% for the GFP channel. The red channel was imaged with an exposure time of 50 ms, Sensitivity of 90 and 561 nm laser power output of 6%. For statistical analysis, the average and standard deviation of three independent FRAP measurements was quantified as described previously (Chan et al, 2012). Data analysis was performed by using Volocity (Perkin Elmer) and processing of images using Adobe Photoshop. All images except Figures 1A and and2A2A and Supplementary Figure S1D were deconvolved to assign out-of-focus light to their point of origin by an iterative deconvolution algorithm and denoised using Volocity software.

Statistical analysis

For FRAP analysis raw data were analysed for each experiment and time point using the Volocity software, which was also used for obtaining the original images. Data for FRAP measurements were transferred to Excel to calculate mean values and standard deviations for all time points of each experiments. For all FRAP experiments, the pre-FRAP signal was set as 100%, the immediate post-value after laser treatment was set as 0% and the subsequent recovery of the fluorescent signal was monitored as the percentage of the pre-FRAP value. Final graphic representation and curve fitting was done using Prism software (Graphpad).

mRNA synthesis

The ORF of Wapl (clone LD29979, BDGP) was amplified by PCR using primers 5′-cgctcaactttggcagatctgaattcagccaccatgTCGCGCTGGGGCAAGAACATCG-3′ and 5′-cactcctgctccggctccCCTGTGGCTGCTGTACGTTTTATAGACC-3′, a blue fluorescent protein tag was amplified using primers 5′-CCACAGGggagccggagcaggagtgagcaagggcgaggagctgttc-3′ and 5′-gtttaggggtaaccagatccgcggccgcTTAgtacagctcgtccatgccgagagtg-3′. Both fragments were ligated in-frame to the pRNA vector using an In-fusion cloning kit (Clontech). In order to ensure translation of the annotated full-length Wapl protein of 1741 amino acids, a mutation using primers 5′-

GCGACTGGCGGGAAAACAAGGAGTACCTGCCACCTCCAC-3′ and 5′-GTGGAGGTGGCAGGTACTCCTTGTTTTCCCGCCAGTCGC-3′ was introduced in the Wapl ORF resulting in the final pRNA-Wapl-BFP vector. Capped mRNAs were synthesized by *in vitro* transcription using the mMessage mMachine T3 kit (Ambion) and purified with RNeasy columns (Qiagen). mRNA was eluted in RNase-free water and injected at 500 ng/μl.

TEV expression and purification

Tagged autoinactivation-resistant TEV protease (2 × NLS-TEV(S219V)-NLS-His6) and catalytically inactive protease (2 × NLS-TEV(C151A)-NLS-His6) were expressed from a pET21D plasmid and purified as previously described (Mishra et al, 2010), except that proteins were stored in injection buffer.

Microinjection of salivary glands

For microinjection experiments, salivary glands from wandering third-instar larvae were dissected in SF9 media, embedded in a low melting agarose (Invitrogen) patch, sandwiched between two coverslips and mounted on a custom made injection plate. Injections were performed using a Scientifica injection system using pre-pulled Femtotip II injection needles (Eppendorf) with TEV protease or catalytically inactive TEV protease (final concentration 1.75 mg/ml in 15 mM potassium phosphate buffer pH 7.4 containing 80 mM KCl, 15 mM NaCl and 5 mM $MgCl_2$). Estimated injection volumes were 5–10% of the volume of one salivary gland cell.

ACKNOWLEDGMENTS

We would like to acknowledge Jean Metson for technical assistance. We thank members of Ilan Davis's lab for discussions and sharing fly stocks and facility, Micron Oxford for excellent help with microscopy, Maurizio Gatti's lab for *wapl*^{C204} mutant flies, Stefan Heidmann's lab for CID-mRFP1 flies and Rad21 antibodies, Juergen Knoblich's lab for H2A-mRFP1 flies stocks, Claudio Sunkel's lab for Smc1 antibodies and all members of Kim Nasmyth's lab for discussions and feedback throughout the project. CSE was supported by a FP7 Marie Curie Intra-European Fellowship. AK and RAO were funded by an ERC grant.

Author contributions: CSE and KN wrote the paper; CSE, AK, RAO, and KN designed the experiments; CSE, AK, and RAO carried out the experiments.

REFERENCES

- Ben-Shahar TR, Heeger S, Lehane C, East P, Flynn H, Skehel M, Uhlmann F (2008) Eco1-dependent cohesin acetylation during establishment of sister chromatid cohesion. Science 321: 563–566

- Chan KL, Roig MB, Hu B, Beckouet F, Metson J, Nasmyth K (2012) Cohesin's DNA exit gate is distinct from its entrance gate and is regulated by acetylation. Cell 150: 961–967
- Ciosk R, Shirayama M, Shevchenko A, Tanaka T, Toth A, Nasmyth K (2000) Cohesin's binding to chromosomes depends on a separate complex consisting of Scc2 and Scc4 proteins. Mol Cell 5: 243–254
- Cuylen S, Metz J, Haering CH (2011) Condensin structures chromosomal DNA through topological links. Nat Struct Mol Biol 18: 894–901
- Dorsett D, Krantz ID (2009) On the molecular etiology of Cornelia de Lange syndrome. Ann NY Acad Sci 1151: 22–37
- Dorsett D, Strom L (2012) The ancient and evolving roles of cohesin in gene expression and DNA repair. Curr Biol 22: R240–R250
- Gandhi R, Gillespie PJ, Hirano T (2006) Human Wapl is a cohesin-binding protein that promotes sister-chromatid resolution in mitotic prophase. Curr Biol 16: 2406–2417
- Gause M, Misulovin Z, Bilyeu A, Dorsett D (2010) Dosage-sensitive regulation of cohesin chromosome binding and dynamics by Nipped-B, Pds5, and Wapl. Mol Cell Biol 30: 4940–4951
- Gimenez-Abian JF, Sumara I, Hirota T, Hauf S, Gerlich D, de la Torre C, Ellenberg J, Peters JM (2004) Regulation of sister chromatid cohesion between chromosome arms. Curr Biol 14: 1187–1193
- Gruber S, Arumugam P, Katou Y, Kuglitsch D, Helmhart W, Shirahige K, Nasmyth K (2006)Evidence that loading of cohesin onto chromosomes involves opening of its SMC hinge. Cell 127: 523–537
- Gruber S, Haering CH, Nasmyth K (2003) Chromosomal cohesin forms a ring. Cell 112: 765–777
- Haering CH, Farcas AM, Arumugam P, Metson J, Nasmyth K (2008) The cohesin ring concatenates sister DNA molecules. Nature 454: 297–301
- Haering CH, Lowe J, Hochwagen A, Nasmyth K (2002) Molecular architecture of SMC proteins and the yeast cohesin complex. Mol Cell 9: 773–788
- Hauf S, Roitinger E, Koch B, Dittrich CM, Mechtler K, Peters JM (2005) Dissociation of cohesin from chromosome arms and loss of arm cohesion during early mitosis depends on phosphorylation of SA2. PLoS Biol 3: e69
- Heidmann D, Horn S, Heidmann S, Schleiffer A, Nasmyth K, Lehner CF (2004) The Drosophila meiotic kleisin C(2)M functions before the meiotic divisions. Chromosoma 113: 177–187
- Hirano T (2006) At the heart of the chromosome: SMC proteins in action. Nat Rev Mol Cell Biol 7: 311–322
- Hu B, Itoh T, Mishra A, Katoh Y, Chan KL, Upcher W, Godlee C, Roig MB, Shirahige K, Nasmyth K (2011) ATP hydrolysis is required for relocating cohesin from sites occupied by its Scc2/4 loading complex. Curr Biol 21: 12–24

- Ivanov D, Schleiffer A, Eisenhaber F, Mechtler K, Haering CH, Nasmyth K (2002) Eco1 is a novel acetyltransferase that can acetylate proteins involved in cohesion. Curr Biol 12: 1–20
- Kueng S, Hegemann B, Peters BH, Lipp JJ, Schleiffer A, Mechtler K, Peters JM (2006) Wapl controls the dynamic association of cohesin with chromatin. Cell 127: 955–967
- Lister LM, Kouznetsova A, Hyslop LA, Kalleas D, Pace SL, Barel JC, Nathan A, Floros V, Adelfalk C, Watanabe Y, Jessberger R, Kirkwood TB, Hoog C, Herbert M (2010) Age-related meiotic segregation errors in mammalian oocytes are preceded by depletion of cohesin and Sgo2. Curr Biol20: 1511–1521
- Liu J, Krantz ID (2008) Cohesin and human disease. Annu Rev Genomics Hum Genet 9: 303–320
- Losada A, Hirano M, Hirano T (1998) Identification of Xenopus SMC protein complexes required for sister chromatid cohesion. Genes Dev 12: 1986–1997
- Losada A, Hirano M, Hirano T (2002) Cohesin release is required for sister chromatid resolution, but not for condensin-mediated compaction, at the onset of mitosis. Genes Dev 16: 3004–3016
- Mannini L, Musio A (2011) The dark side of cohesin: the carcinogenic point of view. Mutat Res728: 81–87
- Mishra A, Hu B, Kurze A, Beckouët F, Farcas AM, Dixon SE, Katou Y, Khalid S, Shirahige K, Nasmyth K (2010) Both interaction surfaces within cohesin's hinge domain are essential for its stable association with chromatin. Curr Biol 20: 279–289
- Nasmyth K (2011) Cohesin: a catenase with separate entry and exit gates? Nat Cell Biol 13: 1170–1177
- Nasmyth K, Haering CH (2005) The structure and function of SMC and kleisin complexes. Annu Rev Biochem 74: 595–648
- Nasmyth K, Haering CH (2009) Cohesin: its roles and mechanisms. Annu Rev Genet 43: 525–528
- Nishiyama T, Ladurner R, Schmitz J, Kreidl E, Schleiffer A, Bhaskara V, Bando M, Shirahige K, Hyman AA, Mechtler K, Peters JM (2010) Sororin mediates sister chromatid cohesion by antagonizing Wapl. Cell 143: 737–749
- Pauli A, Althoff F, Oliveira RA, Heidmann S, Schuldiner O, Lehner CF, Dickson BJ, Nasmyth K (2008) Cell-type-specific TEV protease cleavage reveals cohesin functions in Drosophila neurons.Dev Cell 14: 239–251
- Peters JM, Tedeschi A, Schmitz J (2008) The cohesin complex and its roles in chromosome biology.Genes Dev 22: 3089–3114
- Riedel CG, Katis VL, Katou Y, Mori S, Itoh T, Helmhart W, Galova M, Petronczki M, Gregan J, Cetin B, Mudrak I, Ogris E, Mechtler K, Pelletier L, Buchholz F, Shirahige K, Nasmyth K (2006)Protein phosphatase 2A protects centromeric sister chromatid cohesion during meiosis I. Nature 441: 53–61
- Rowland BD, Roig MB, Nishino T, Kurze A, Uluocak P, Mishra A, Beckouet F, Underwood P, Metson J, Imre R, Mechtler K, Katis VL, Nasmyth K (2009) Building

sister chromatid cohesion: smc3 acetylation counteracts an antiestablishment activity. Mol Cell 33: 763–774

- Schuh M, Lehner CF, Heidmann S (2007) Incorporation of Drosophila CID/CENP-A and CENP-C into centromeres during early embryonic anaphase. Curr Biol 17: 237–243
- Shintomi K, Hirano T (2009) Releasing cohesin from chromosome arms in early mitosis: opposing actions of Wapl-Pds5 and Sgo1. Genes Dev 23: 2224–2236
- Sumara I, Vorlaufer E, Stukenberg PT, Kelm O, Redemann N, Nigg EA, Peters JM (2002) The dissociation of cohesin from chromosomes in prophase is regulated by Polo-like kinase. Mol Cell 9: 515–525
- Unal E, Heidinger-Pauli JM, Kim W, Guacci V, Onn I, Gygi SP, Koshland DE (2008) A molecular determinant for the establishment of sister chromatid cohesion. Science 321: 566–569 Verni F, Gandhi R, Goldberg ML, Gatti M (2000) Genetic and molecular analysis of wings apart-like (wapl), a gene controlling heterochromatin organization in Drosophila melanogaster. Genetics 154: 1693–1710
- Waizenegger I, Hauf S, Meinke A, Peters JM (2000) Two distinct pathways remove mammalian cohesin from chromosome arms in prophase and from centromeres in anaphase. Cell 103: 399–410
- Xu Z, Cetin B, Anger M, Cho US, Helmhart W, Nasmyth K, Xu W (2009) Structure and function of the PP2A-shugoshin interaction. Mol Cell 35: 426–441

FIGURE LEGENDS

Figure 1: Cohesin localization and dynamics in non-dividing salivary gland cells of *Drosophila melanogaster*. (**A**) Rad21(TEV)-GFP localizes to specific bands on polytene chromosomes of *Drosophila melanogaster* in a wild-type background. Chromatin is marked as H2Av-mRFP1. (**B**) Rad21(TEV)-GFP at specific chromosome sites is dynamic as measured by FRAP. (**C**) Statistical analysis of three independent Rad21(TEV)-GFP FRAP measurements in a wild-type background (data represented as mean±s.d.). RFI, relative fluorescence intensity. (**D**) Cleavage of cohesin's kleisin subunit Rad21(TEV)-GFP by microinjected active TEV protease in wild-type salivary gland cells. Scale bars represent a length of 5 µm.

Figure 2: Cohesin dynamics in non-dividing salivary gland cells depend on Wapl. (**A**) Rad21(TEV)-GFP localizes to specific bands on polytene chromosomes of *Drosophila melanogaster* in a $wapl^{C204}$ mutant background. Chromatin is marked as H2Av-mRFP1. (**B**) Rad21(TEV)-GFP turnover in a $wapl^{C204}$ mutant background as measured by FRAP. (**C**) Statistical analysis of three independent Rad21(TEV)-GFP FRAP measurements in a wild-type and $wapl^{C204}$ mutant background (data

represented as mean±s.d.). RFI, relative fluorescence intensity. (**D**) Microinjection of full-length Wapl-BFP mRNA in *wapl*^{C204} Rad21(TEV)-GFP Rad21^{ex} H2Av-mRFP1 salivary gland cells. A non-injected cell (left) and a Wapl-BFP mRNA injected cell (right) are depicted. Chromatin is marked as H2Av-mRFP1. (**E**) Cleavage of cohesin's kleisin subunit Rad21(TEV)-GFP by microinjected active TEV protease in *wapl*^{C204} mutant salivary gland cells. Scale bars represent a length of 5 µm.

Figure 3: A GAL4-inducible and TEV-cleavable Smc3-Rad21-GFP fusion protein of cohesin localizes to specific chromatin sites in salivary glands of *Drosophila melanogaster*. (**A**) Construction of transgenic fly lines expressing a GAL4-inducible and TEV-cleavable Smc3-Rad21-GFP fusion protein. Smc3-Rad21-GFP fusion proteins alone or in combination with TEV protease are expressed from GAL4-inducible promoters that are activated by a heat shock-inducible GAL4 driver transgene. (**B**) Western blot showing expression of Smc3-Rad21-GFP using a heat shock-inducible GAL4 driver transgene. Third-instar larvae were heat shocked for 30 min at 37°C followed by a 7 h incubation at 25°C. (**C**) Smc3-Rad21-GFP is cleaved in presence of co-expressed TEV protease in salivary gland cells. Both Smc3-Rad21-GFP and TEV protease are expressed from a GAL4-inducible promoter that is activated via a heat shock-inducible GAL4 driver transgene. Third-instar larvae were heat shocked for 2 min at 37°C followed by a 2 h incubation at 25°C. In (**B**, **C**), the following antibodies were used: guinea-pig α-Rad21 (1:5000) (Heidmann et al, 2004), α-Smc1 (1:2000), and mouse α-tubulin (DM1A) (1:7500). HRP-linked guinea-pig (1:15 000), mouse (1:5000), and rat (1:5000) secondary antibodies were detected by Enhanced Chemi-Luminescence (ECL). (**D**) Smc3-Rad21-GFP fusion protein localizes to specific bands on salivary gland polytene chromosomes of *Drosophila melanogaster.* Chromatin is marked as H2Av-mRFP1. Scale bars represent a length of 5 µm.

Figure 4: Cohesin dynamics in non-dividing salivary gland cells depend on opening of the Smc3-Rad21 gate. (**A**) Smc3-Rad21-GFP turnover measured by FRAP with or without co-expression of TEV protease from a GAL4-inducible transgene. (**B**) Statistical analysis of three independent Smc3-Rad21-GFP FRAP measurements in the presence or absence of co-expressed TEV protease (data represented as mean±s.d.). RFI, relative fluorescence intensity. Scale bars represent a length of 5 µm.

Figure 5: Cleaving the polypeptide linking Smc3's NBD to kleisin's N-terminus triggers Wapl-dependent release. (**A**) Microinjection of active TEV protease into Smc3-Rad21-GFP-expressing salivary glands in a wild-type background. (**B**) Microinjection of inactive TEV protease into Smc3-Rad21-GFP-expressing salivary glands in a wild-type background. (**C**) Microinjection of active TEV protease into Smc3-Rad21-GFP-expressing salivary glands in a $wapl^{C204}$ mutant background. Scale bars represent a length of 5 µm.

Figure 6: Cohesin removal from chromosome arms in prophase depends on Wapl and on opening of the Smc3-Rad21 gate. (**A**) Rad21(TEV)-GFP localization in wild-type prophase neuroblasts. (**B**) Cohesin's kleisin subunit Rad21 localizes to peri-centromeric regions in a wild-type neuroblast. Images of Rad21-GFP and CID-mRFP1 in a Rad21 excision background are shown. (**C**) Rad21(TEV)-GFP localization in$wapl^{C204}$ mutant prophase neuroblasts. (**D**) Smc3-Rad21-GFP fusion proteins localize to chromosome arms of prophase neuroblasts. For each experiment, brain tissues were dissected from third-instar larvae with the respective genotype after a short heat shock and recovery time to allow Smc3-Rad21-GFP expression. Larval brains were mounted in Schneider media on poly-lysine coated slides and covered by a membrane and a layer of oil. Neuroblasts that had undergone nuclear envelope breakdown but not metaphase-to-anaphase transition was imaged using spinning disk confocal microscopy. Scale bars represent a length of 2.5 µm.

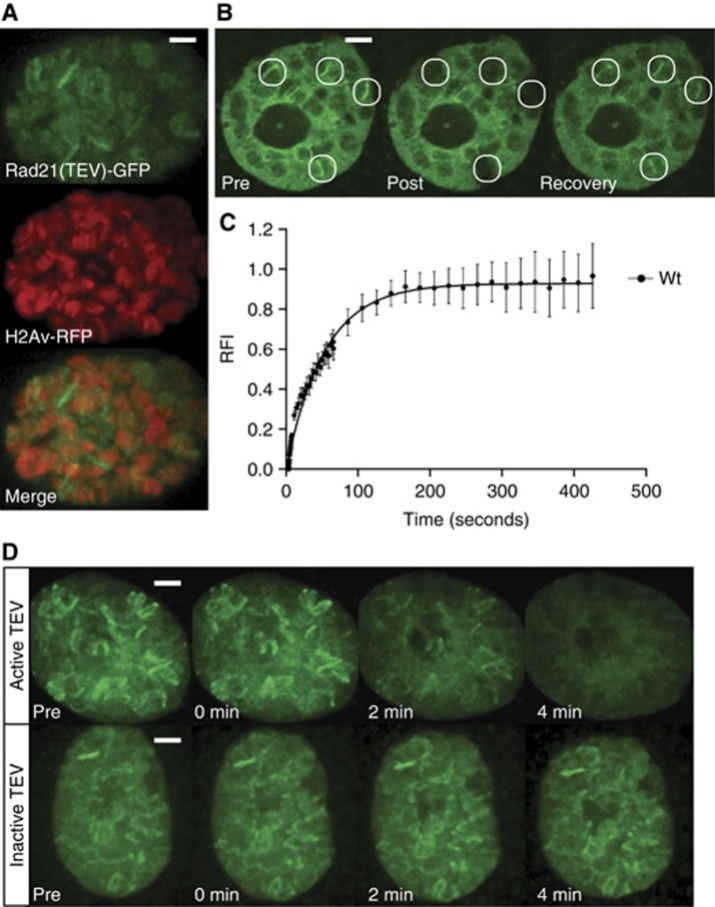
A
Rad21(TEV)-GFP
H2Av-RFP
Merge
B
Pre
Post
Recovery
C
RFI
Time (seconds)
Wt
D
Active TEV
Inactive TEV
Pre
0 min
2 min
4 min

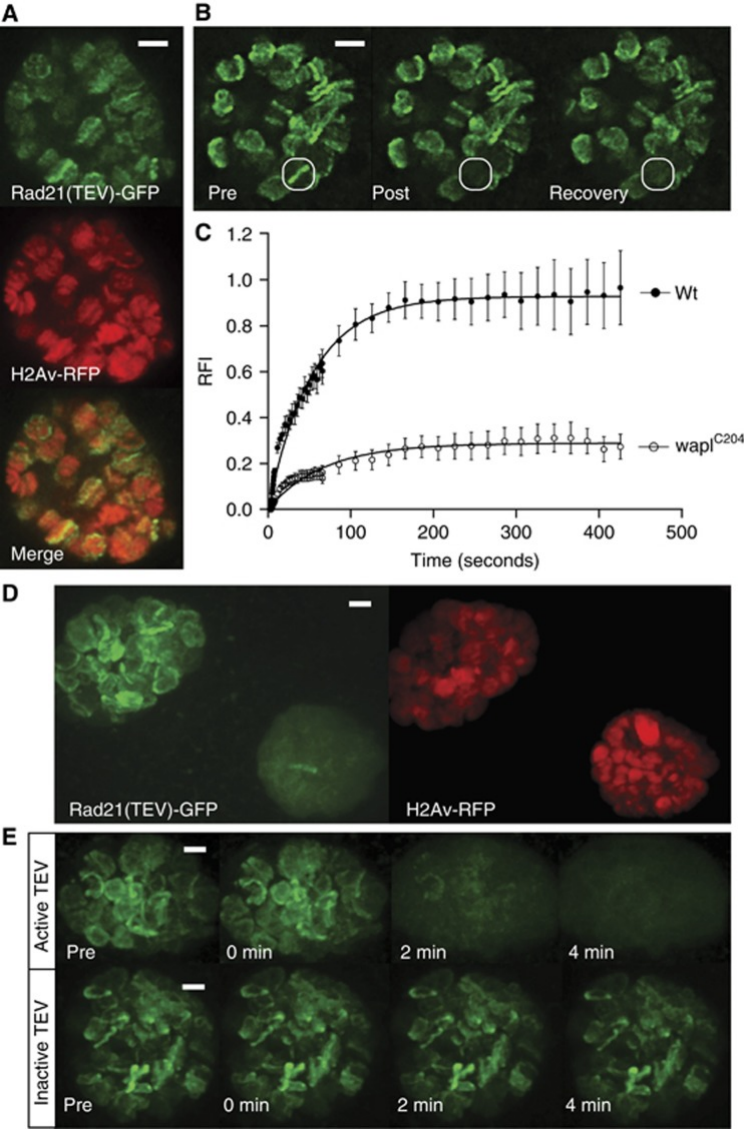
A
Rad21(TEV)-GFP
H2Av-RFP
Merge
B
Pre
Post
Recovery
C
RFI
Time (seconds)
Wt
wapl^C204
D
Rad21(TEV)-GFP
H2Av-RFP
E
Active TEV
Inactive TEV
Pre
0 min
2 min
4 min

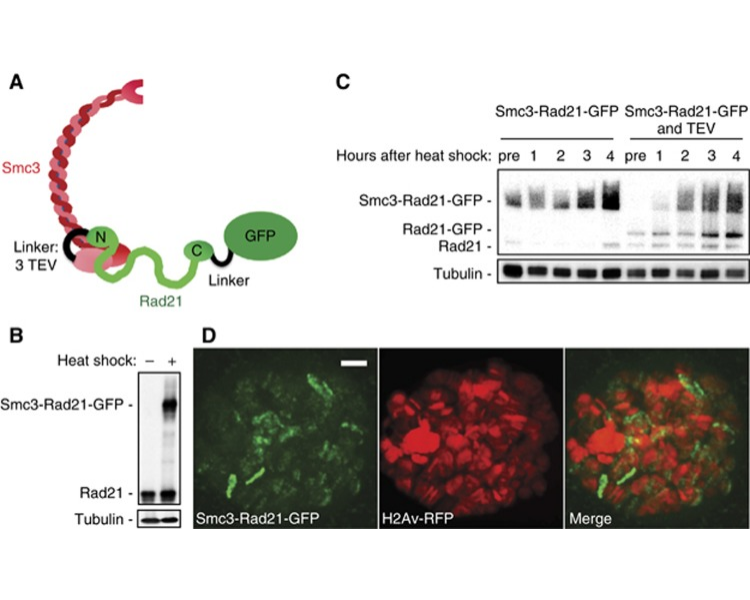
A
Smc3
N
Linker:
3 TEV
C
GFP
Linker
Rad21
B
Heat shock: – +
Smc3-Rad21-GFP -
Rad21 -
Tubulin -
C
Smc3-Rad21-GFP
Smc3-Rad21-GFP and TEV
Hours after heat shock: pre 1 2 3 4 pre 1 2 3 4
Smc3-Rad21-GFP -
Rad21-GFP -
Rad21 -
Tubulin -
D
Smc3-Rad21-GFP
H2Av-RFP
Merge

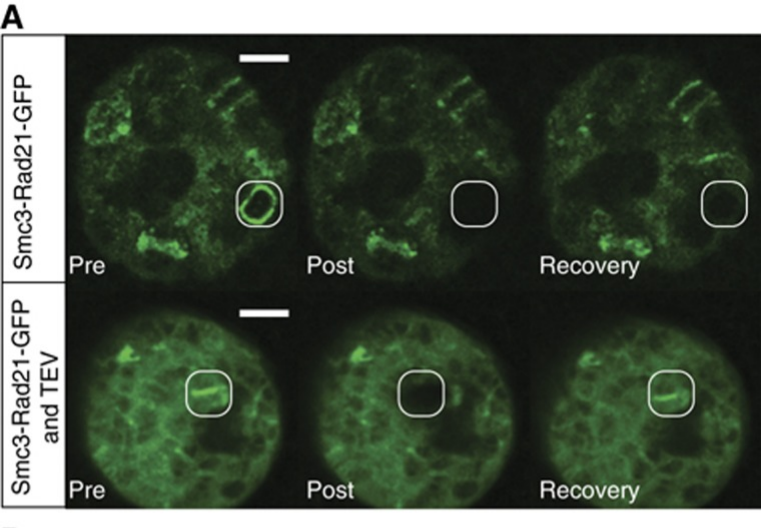
A
Smc3-Rad21-GFP
Pre
Post
Recovery
Smc3-Rad21-GFP and TEV
Pre
Post
Recovery

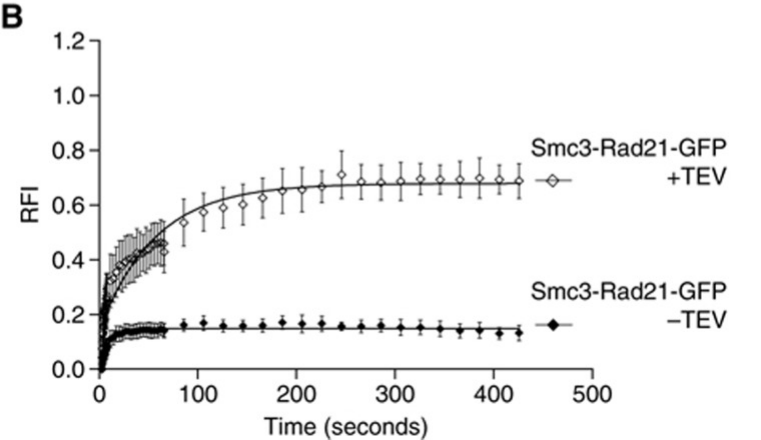
B
RFI
1.2
1.0
0.8
0.6
0.4
0.2
0.0
0
100
200
300
400
500
Time (seconds)
Smc3-Rad21-GFP
+TEV
Smc3-Rad21-GFP
–TEV

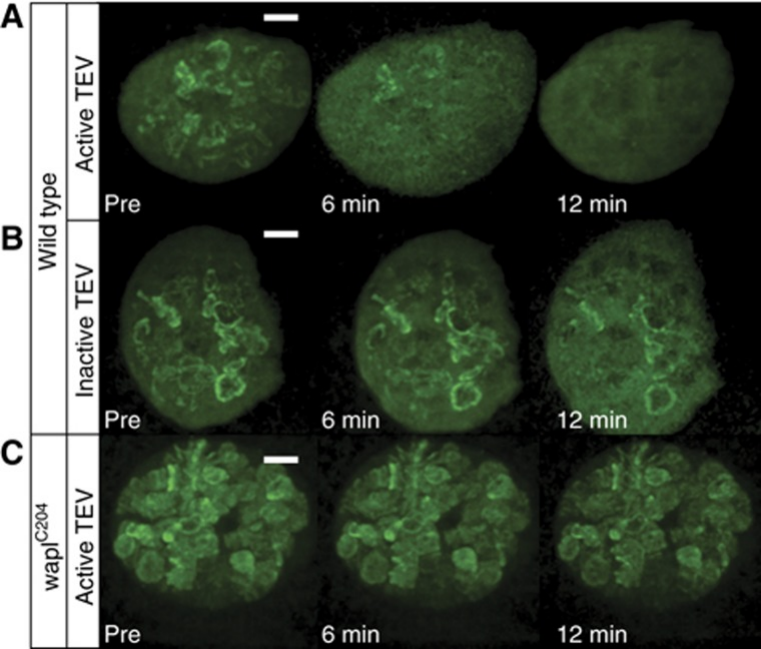
A
Wild type
Active TEV
Pre
6 min
12 min
B
Inactive TEV
Pre
6 min
12 min
C
wapl^{C204}
Active TEV
Pre
6 min
12 min

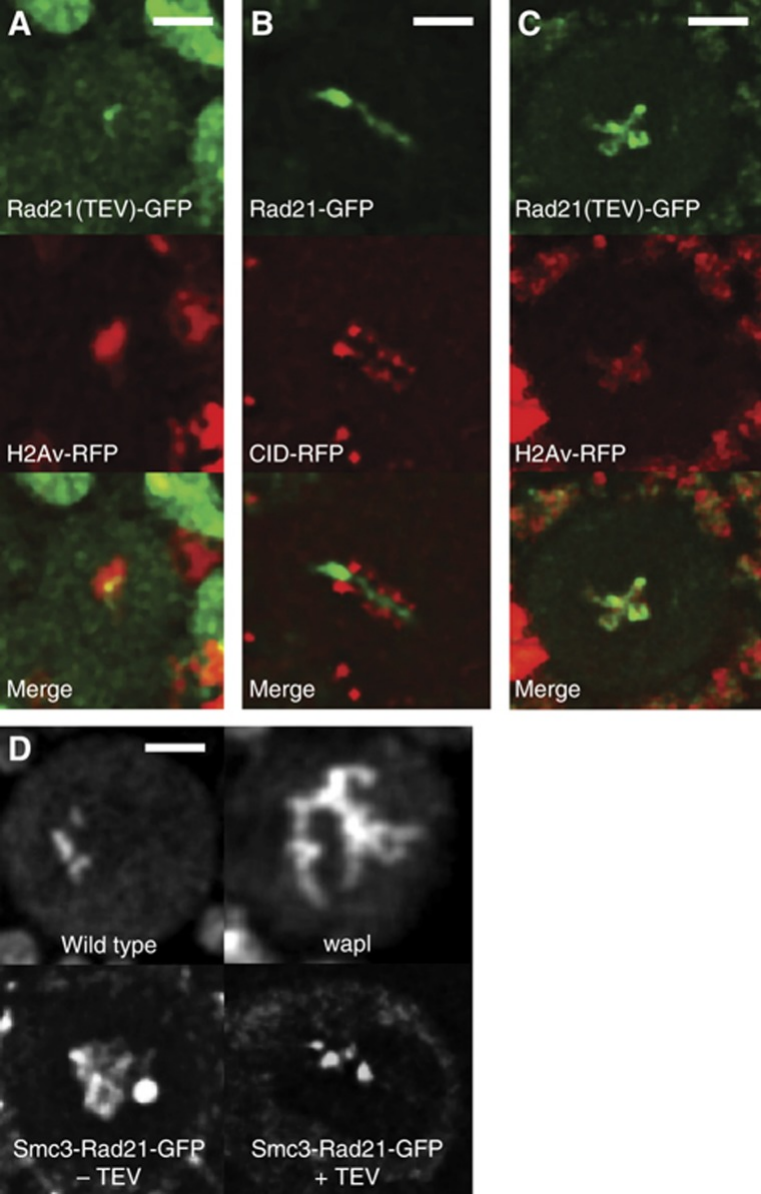
A
Rad21(TEV)-GFP
H2Av-RFP
Merge
B
Rad21-GFP
CID-RFP
Merge
C
Rad21(TEV)-GFP
H2Av-RFP
Merge
D
Wild type
wapl
Smc3-Rad21-GFP
– TEV
Smc3-Rad21-GFP
+ TEV

EMBO Journal

Supplementary Information

Disengaging the Smc3/kleisin interface releases cohesin from Drosophila chromosomes during interphase and mitosis

Christian S. Eichinger, Alexander Kurze, Raquel A. Oliveira and Kim Nasmyth

SUPPLEMENTARY TABLE S1: Fly stocks

Genotype	Reference
;;pTubulin-Rad21-GFP	This study and (Oliveira et al, in preparation)
;;pTubulin-Rad21(550-3TEV)-GFP	This study and (Oliveira et al, in preparation)
;;pPolyubiquitin-H2Av-mRFP1	(Schuh et al, 2007)
;;pTubulin-Rad21(550-3TEV)-GFP, $Rad21^{ex15}$, pPolyubiquitin-H2Av-mRFP1/TM3	This study
;;pTubulin-GFP-Smc3/TM3	This study
$wapl^{C204}$/FM7;;	(Verni et al, 2000)
$wapl^{C204}$/FM7i, Actin-GFP;;Rad21(550-3TEV)-GFP, $Rad21^{ex15}$, pPolyubiquitin-H2Av-mRFP1/TM3	This study
;;pUAS-Smc3-(3TEV)-Rad21-GFP	This study
;;pUAS-NLS-TEV-v5-NLS2	(Pauli et al, 2008)
;;hsGAL4	(Pauli et al, 2008)
;;pUAS-NLS-TEV-v5-NLS2, hsGAL4	(Pauli et al, 2008)
;Cid-mRFP1;	(Schuh et al, 2007)
;;pTubulin-Rad21-GFP, $Rad21^{ex15}$, pPolyubiquitin-H2Av-mRFP1	This study
;Cid-mRFP1;pTubulin-Rad21-GFP, $Rad21^{ex15}$	This study and (Oliveira et al, in preparation)

SUPPLEMENTARY FIGURE:

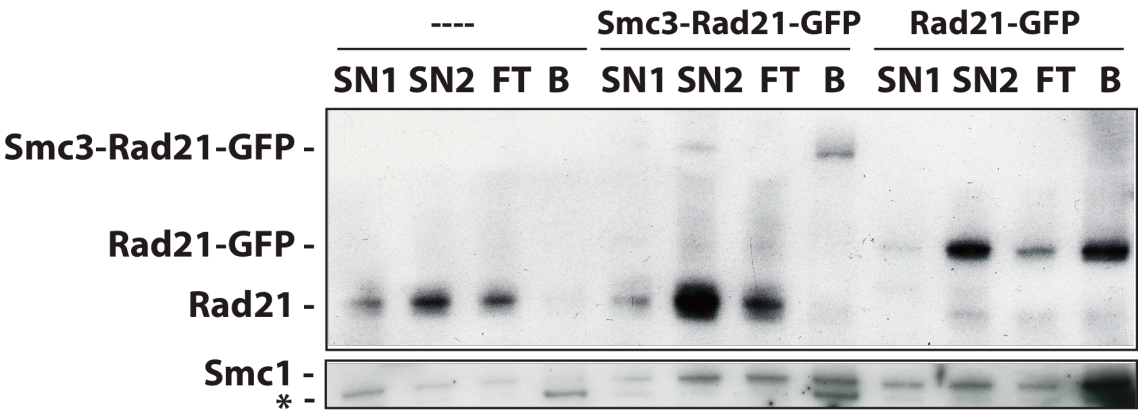

Supplementary Figure S1: Co-Immunoprecipitation of Smc3-Rad21-GFP

Chromatin-bound Smc3-Rad21-GFP fusion protein interacts with endogenous Smc1 but not with endogenous Rad21. Immunoprecipitation of Smc3-Rad21-GFP was carried out using anti-GFP beads (Chromotek) from larval extracts after heat-shock treatment (5 min at 37°C, 2 hours at 25°C). Lysates of 30 larvae were prepared by squashing in lysis buffer (50mM Tris/Cl pH7.5, 250mM NaCl, 1mM $MgCl_2$, 0.5% NP40 and Roche protease inhibitor mix) and run on a 30% sucrose gradient – the yellow top layer of the gradient presents the supernatant 1 fraction (SN1). Chromatin-bound proteins were then released from the remaining pellet fraction by addition of Benzonase in lysis buffer (60 minutes on ice), sonicated (40% amplitude, 5 seconds) and centrifuged in order to obtain the supernatant 2 fraction (SN2). SN2 was directly added to equilibrated GFP-Trap beads (Chromotek, Planegg-Martinsried, Germany) following manufacturer's instructions. All washes as well as equilibration of GFP-Trap beads were done using wash buffer (50mM Tris/Cl pH7.5, 250mM NaCl and Roche protease inhibitor mix). The flow-through of protein material not binding to the beads was collected (FT). The fraction of proteins bound to the beads (B) was eluted from GFP-Trap beads by boiling in protein sample buffer. The four fractions (SN1, SN2, FT and B) were loaded on NuPAGE 4-12% Bis/Tris gels and run using MES buffer according to manufacturer's instructions (Novex/LifeTechologies, Paisley, UK). For detection of proteins, antibodies against Rad21 (Stefan Heidmann lab) and Smc1 (Claudio Sunkel lab) were used. The asterisk marks a non-specific band.

SUPPLEMENTARY MOVIES S1 to S13

Movie S1: FRAP movie of individual Rad21(TEV)-GFP bands in wildtype

Movie S2: FRAP movie of GFP-Smc3 in wildtype

Movie S3: Rad21(TEV)-GFP movie in wildtype after injection of active TEV

Movie S4: Rad21(TEV)-GFP movie in wildtype after injection of inactive TEV

Movie S5: FRAP movie of Rad21(TEV)-GFP in $wapl^{C204}$ after injection of Wapl-BFP

Movie S6: Rad21(TEV)-GFP movie in $wapl^{C204}$ after injection of active TEV

Movie S7: Rad21(TEV)-GFP movie in $wapl^{C204}$ after injection of inactive TEV

Movie S8: Smc3-Rad21-GFP movie after injection of active TEV

Movie S9: Smc3-Rad21-GFP movie after injection of inactive TEV

Movie S10: Smc3-Rad21-GFP movie in $wapl^{C204}$ after injection of active TEV

Movie S11: FRAP movie of Smc3-Rad21-GFP in $wapl^{C204}$ after injection of active TEV

Movie S12: Neuroblast movie of wildtype *Rad21(TEV)-GFP* $Rad21^{ex}$ *H2Av-mRFP1*

Movie S13: Neuroblast movie of $wapl^{C204}$ *Rad21(TEV)-GFP* $Rad21^{ex}$ *H2Av-mRFP1*

The time-scale of each movie is presented as hh:mm:ss.ms.

SUPPLEMENTARY REFERENCES

Pauli A, Althoff F, Oliveira RA, Heidmann S, Schuldiner O, Lehner CF, Dickson BJ, Nasmyth K (2008) Cell-type-specific TEV protease cleavage reveals cohesin functions in Drosophila neurons. *Dev Cell* **14**(2)**:** 239-251

Schuh M, Lehner CF, Heidmann S (2007) Incorporation of Drosophila CID/CENP-A and CENP-C into centromeres during early embryonic anaphase. *Curr Biol* **17**(3)**:** 237-243

Verni F, Gandhi R, Goldberg ML, Gatti M (2000) Genetic and molecular analysis of wings apart-like (wapl), a gene controlling heterochromatin organization in Drosophila melanogaster. *Genetics* **154**(4)**:** 1693-1710